Radiation Protection Dosimetry (2018), pp. 1–9 doi:10.1093/rpd/ncy166

ANALYTICAL MODEL TO ESTIMATE EQUIVALENT DOSE FROM INTERNAL NEUTRONS IN PROTON THERAPY OF CHILDREN WITH INTRACRANIAL TUMORS

Kyle J. Gallagher[1,2] and Phillip J. Taddei[3,4,*]
[1]Oregon Health and Science University, Portland, OR, USA
[2]Oregon State University, Corvallis, OR, USA
[3]American University of Beirut Medical Center, Beirut, Lebanon
[4]Department of Radiation Oncology, University of Washington School of Medicine, 1959 NE Pacific Street, Box 356043, Seattle, WA 98195, USA

*Corresponding author: ptaddei@uw.edu

Received 5 May 2018; revised 15 August 2018; editorial decision 16 August 2018; accepted 27 August 2018

This study developed a computationally efficient and easy-to-implement analytical model to estimate the equivalent dose from secondary neutrons originating in the bodies ('internal neutrons') of children receiving intracranial proton radiotherapy. A two-term double-Gaussian mathematical model was fit to previously published internal neutron equivalent dose per therapeutic absorbed dose versus distance from the field edge calculated using Monte Carlo simulations. The model was trained using three intracranial proton fields of a 9-year-old girl. The resulting model was tested against two intracranial fields of a 10-year-old boy by comparing the mean doses in organs at risk of a radiogenic cancer estimated by the model versus those previously calculated by Monte Carlo. On average, the model reproduced the internal neutron organ doses in the 10-year-old boy within 13.5% of the Monte Carlo at 3–10 cm from the field edge and within a factor of 2 of the Monte Carlo at 10–20 cm from the field edge. Beyond 20 cm, the model poorly estimated H/D_{Rx}, however, the values were very small, at <0.03 mSv Gy^{-1}.

INTRODUCTION

By the end of 2016, ~150 000 patients had been treated with proton radiotherapy worldwide[1]. For treating some pediatric cancers, particularly those of the central nervous system, proton therapy is becoming the modality of choice[2]. Two of the main motivations of proton therapy for children are to mitigate acute effects and to lessen the risk or detriment of late effects in organs in or near the treatment fields.

For children with intracranial or other tumors, among the late effects of greatest concern are radiation-induced subsequent malignant neoplasms (SMNs) because of their associated morbidity and mortality. For example, investigators in the Childhood Cancer Survivor Study found that mortalities 20 years after the initial diagnosis were attributed primarily to SMNs[3, 4]. SMNs emerge not only inside but outside the treatment field, where doses from stray (i.e. non-therapeutic) radiation dominate[5, 6]. Therefore, to estimate and ultimately design treatments to minimize these effects, it is essential to quantify the dose from stray radiation in organs and tissues at risk for SMNs.

Stray neutrons that are generated in proton therapy have enhanced damage capability and higher relative biological effectiveness (RBE) to produce detrimental effects—e.g. carcinogenesis—than protons, photons and electrons[7]. These neutrons can be produced in the bodies of patients ('internal neutrons') or in the treatment apparatus ('external neutrons'). Because they focus on accuracy within the treatment fields, modern treatment planning systems (TPSs) in the proton therapy clinic do not account for the equivalent dose from stray neutrons. Detailed Monte Carlo simulations have been developed to quantify the equivalent dose from stray neutrons in certain environments[8–15]. However, because it is computationally expensive, Monte Carlo has failed to be universally embraced, in particular, for estimating stray radiation doses. Consequently, rudimentary analytical models may be advantageous for estimating stray radiation doses that are sufficiently accurate and computationally inexpensive. Much research has been dedicated to developing an analytical model for external neutrons in proton therapy[16–20]. In contrast to external neutron models, which are highly dependent on the treatment apparatus and environment, an internal neutron model is independent of the facility and can be applied universally. At the time of this writing, an analytical model for estimating dose from internal neutrons in proton therapy had not been developed.

The purpose of this study was to develop a computationally efficient analytical model to estimate the equivalent dose from internal neutrons in proton therapy of children with intracranial tumors. To

train and test the model, available Monte Carlo simulation data were used from the literature for a 9-year-old girl and a 10-year-old boy who received passively scattered proton radiotherapy for brain tumors[11, 12]. The internal neutron model was trained using the Monte Carlo dataset of the girl, and, as a first test, the model was applied to the fields of the boy. This model was independent of treatment facility but was not intended to be universal for all proton therapy cases. Instead, the most common pediatric proton therapy treatment (i.e. intracranial tumors) was selected which comprises ~40% of all pediatric proton treatments in the USA[21].

MATERIALS AND METHODS

Prescription and treatment planning

The treatment plans of the previous study for the 9-year-old girl and the 10-year-old boy called for intracranial boost fields to deliver a total of 23.4 Gy-RBE[22], or 21.3 Gy of absorbed dose, in the clinical target volume using a passive scattering treatment unit. Their relevant field characteristics are summarized in Table 1. Because the girl's plan contained three fields and the boy's plan contained two fields and each field contributed equally, the prescribed absorbed dose for each field, D_{Rx}, was 7.09 Gy for the girl and 10.64 Gy for the boy. These treatment fields were similar to those of patients treated for low-grade localized brain tumors, such as astrocytomas, ependymomas and gliomas. Information regarding the computed tomography (CT) simulations, treatment plans, and Monte Carlo techniques were published previously[11, 12]. The data for the 9-year-old girl were used to train the model, and the data for the 10-year-old boy were used to test the model.

Distance from the field edge

The distance between the field edge (i.e. 50% isodose surface) and each out-of-field voxel, r, was determined by the following steps. First, data in the Digital Imaging and Communications in Medicine (DICOM) standard format were read into commercial software (version R2016b, MATLAB, The MathWorks, Inc., Natick, MA) using in-house scripts. Next, for each field, the field edge was defined as the Cartesian coordinates corresponding to voxels with therapeutic absorbed dose, D, between $0.5 \times D_{Rx} - 0.1$ Gy and $0.5 \times D_{Rx} + 0.1$ Gy. Then, voxels in which D was $<0.5 \times D_{Rx}$ (3.55 Gy for the girl and 5.32 Gy for the boy) were defined as out-of-field. The Cartesian coordinates of these out-of-field voxels were recorded. Finally, r was calculated as the shortest distance between each out-of-field voxel and the field edge using the Euclidean norm.

Training of the analytical model

The proposed analytical model was trained using the previously reported Monte Carlo data for the 9-year-old girl. The model was separated into components for lower energy and higher energy beams—the lower energy component for fields having nominal energy (i.e. energy of the most distal Bragg peak of a multi-energetic beam), E, ≤160 MeV and the higher energy component for fields having E >160 MeV. The components were split at E of 160 MeV because this is a mid-range E for treating pediatric tumors. The lower energy and higher energy components were trained separately by data from intracranial proton fields that were lower energy and higher energy, respectively. Each component was a double-Gaussian function that related the voxel's internal neutron equivalent dose, H, (in mSv) per D_{Rx} (in Gy) as a function of r (cm),

$$H/D_{Rx} = \begin{cases} \dfrac{\alpha_{L1}}{\sqrt{2\pi\sigma_{L1}^2}} e^{-\frac{(r-\mu_{L1})^2}{2\sigma_{L1}^2}} + \dfrac{\alpha_{L2}}{\sqrt{2\pi\sigma_{L2}^2}} e^{-\frac{(r-\mu_{L2})^2}{2\sigma_{L2}^2}}, & E \le 160 \text{ MeV} \\ \dfrac{\alpha_{H1}}{\sqrt{2\pi\sigma_{H1}^2}} e^{-\frac{(r-\mu_{H1})^2}{2\sigma_{H1}^2}} + \dfrac{\alpha_{H2}}{\sqrt{2\pi\sigma_{H2}^2}} e^{-\frac{(r-\mu_{H2})^2}{2\sigma_{H2}^2}}, & E > 160 \text{ MeV} \end{cases} \quad (1)$$

where the lower (L) and higher (H) energy components denoted the means, μ_1 and μ_2, standard deviations, σ_1 and σ_2, and amplitudes, α_1 and α_2, of each Gaussian term. In the past, the double-Gaussian function has been used to characterize lateral profiles in radiotherapy—e.g. external neutron equivalent dose produced in passively scattered proton therapy[20], spot scanning proton absorbed dose[23], and out-of-field absorbed doses in photon therapy[8, 24, 25]. In this study, the Gaussian terms of the model did not

Table 1. Proton beam characteristics for the intracranial boost fields for the 9-year-old girl and 10-year-old boy in the previous study[11, 12].

	Girl			Boy	
Pre-nozzle proton energy (MeV)	160	180	160	160	140
Beam orientation	LPO	PA	RPO	LPO	LL
Gantry angle (°)	97	180	263	130	90
Range in patient (cm of water H_2O)	12.0	13.5	12.0	11.3	9.2
SOBP width (cm)	8	8	8	7	6
Collimated field, major axis (cm)	6.6	7.0	6.3	11.8	11.6
Collimated field, minor axis (cm)	6.3	6.3	6.3	5.5	5.4
Air gap (cm)	23	29	23	2	2
Aperture thickness (cm)	4	6	4	4	4

LPO, left posterior oblique; PA, posterior anterior; RPO, right posterior oblique; LL, left lateral.

describe a physical phenomenon but were purely empirical.

To train the model, least squares fitting was performed on each component using the commercial software and in-house scripts, with all six fitting parameters varying to minimize the root mean square deviation, *RMSD*, in H/D_{Rx}. Data for beams having nominal energies ≤160 MeV (i.e. right posterior oblique and left posterior oblique) were concatenated to create one dataset for the fitting procedure. Only voxels with $r \leq 49$ cm were used to fit the model parameters for the following reasons. First, beyond this imposed upper limit, a large percentage of voxels were located at or near the girl's skin in her arms. Near the skin, volume averaging between tissue and air caused an artificial overestimation of H/D_{Rx}. Second, before the artificial overestimation from volume averaging, the H/D_{Rx} values were very small (on average <0.009 mSv Gy^{-1}) at 49 cm from the field edge as shown in Figures 1 and 2.

The following further considerations were made in training the model. To determine where to apply the model, new observations were made of the previously published Monte Carlo results. Specifically, for each field, equivalent dose per D_{Rx} versus r were compared for each type of radiation, i.e. therapeutic protons, internal neutrons, and external neutrons, which were determined from the previous Monte Carlo simulations. For protons, the RBE-weighted dose (mGy-RBE) per D_{Rx} was used instead of equivalent dose to be consistent with clinical practice. The Monte Carlo data were averaged into 1-mm bins of r. A lower limit of application of the model was defined at $r = 3$ cm, where H/D_{Rx} from internal neutrons in mSv Gy^{-1} exceeded 25% of the RBE-weighted dose from therapeutic protons per D_{Rx} in mGy-RBE Gy^{-1}.

Testing the analytical model

The fitted analytical model was tested against the previously reported internal neutron Monte Carlo data of the 10-year-old boy in the following manner. H/D_{Rx} was calculated in each out-of-field voxel of the boy's CT image set based on the model and fitting parameters that were calculated in the training of the model. Out-of-field voxels and their distances from the field edge were defined in the same method as with the girl. This analytical model result was then compared to the Monte Carlo result by averaging, as a figure of merit, each voxel of the out-of-field H/D_{Rx} in organs and tissues at risk for a radiogenic SMN, T, H_T/D_{Rx}. For this out-of-field dose comparison, only organs beyond 3 cm from the field edge were considered. T were selected based on the recommendations of the International Commission on Radiological Protection (ICRP)[26]. These T comprised the esophagus, lungs, stomach, liver, colon (which included the rectum), bladder, gonads and the thyroid.

RESULTS

New observations of previously published Monte Carlo results

The Monte Carlo data from the previous study for the $E = 160$ MeV proton beams and the $E = 180$ MeV beam of the girl are plotted in Figure 1. For the 160 and 180 MeV beams, therapeutic protons contributed the most to the total dose for $0 < r \leq 3.55$ cm and $0 < r \leq 3.85$ cm, respectively. Beyond these distances, external neutrons were the main contributors. Beyond $r = 3$ cm, H/D_{Rx} values from internal neutrons in mSv Gy^{-1} exceeded 25% of the RBE-weighted dose from therapeutic protons per D_{Rx} in mGy-RBE Gy^{-1}. For $r >$ 49 cm, where all voxels were from the girl's arms, volume averaging strongly influenced the H/D_{Rx} data. For this reason, only data for $r \leq 49$ cm were used to fit the model parameters. Thus, the applicable region of the model was 3 cm $< r \leq 49$ cm.

Training of the analytical model

The parameters of the analytical model were fit to the measured data separately for each component.

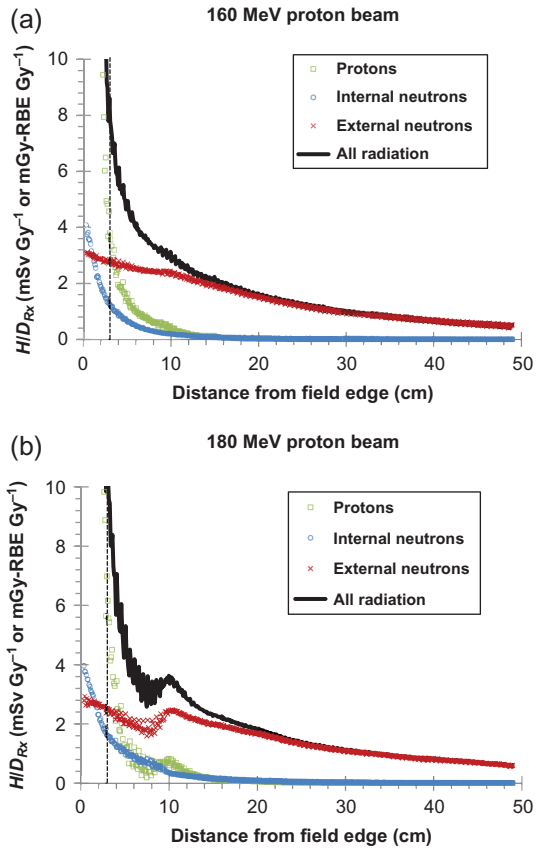

Figure 1. Equivalent dose per prescribed absorbed dose from therapeutic protons (green squares), internal neutrons (blue circles), external neutrons (red crosses), and all radiation types (black line) for the Monte Carlo data that trained the lower energy component (**a**) and higher energy component (**b**) of the model. Instead of equivalent dose, the RBE-weighted dose per D_{Rx} was presented for protons to be consistent with clinical practice. For clarity in viewing, the Monte Carlo data were averaged in 0.1-mm bins. The Monte Carlo data were from reference[11]. A dashed line was drawn at 3 cm from the field edge to indicate where the H/D_{Rx} values from internal neutrons in mSv Gy^{-1} exceeded 25% of the RBE-weighted dose from therapeutic protons per D_{Rx} in mGy-RBE Gy^{-1}.

Parameter and RMSD values are listed in Table 2. The best fits resulted in the mean of each Gaussian term less than zero and both narrow and wide standard deviations. The RMSD values were small, at <0.23 mSv Gy^{-1} or 11.3 mSv for a 54 Gy-RBE (i.e. 49.1 Gy) treatment, corresponding to <5.8% of the average H/D_{Rx} near the field edge.

For the training data of the girl's fields, the analytical model is plotted in Figure 2 along with the corresponding Monte Carlo data for internal neutron H/D_{Rx}. For easier viewing, the plots are shown on linear–linear and logarithmic–linear axes, and the Monte Carlo data were averaged into bins. The Monte Carlo data matched the analytical model very well. For 3 cm < r < 10 cm, the analytical model followed the Monte Carlo H/D_{Rx} closely as they decreased from 1.21 to 0.19 mSv Gy^{-1} and 1.63 to 0.40 mSv Gy^{-1} for the lower and higher energy components, respectively. For 20 cm < r < 41 cm, both the analytical model and Monte Carlo data reduced by a factor of 7 from 0.05 to 0.007 mSv Gy^{-1} and 0.09 to 0.013 mSv Gy^{-1} for the lower energy and higher energy components, respectively. For $r \geq$ 41 cm, the higher energy component underestimated the Monte Carlo data. However, H/D_{Rx} was very small beyond 41 cm (<0.014 mSv Gy^{-1}), implying that the accuracy of the model was less critical in that region compared to r < 41 cm. Everywhere in the applicable region of the model, 3 < $r \leq$ 49 cm, the higher energy component H/D_{Rx} was at least 30% higher than the lower energy component H/D_{Rx}.

Testing of the analytical model

For the testing data of the boy's fields, the analytical model estimation is plotted in Figure 3 against the Monte Carlo data for internal neutrons. From 3 cm to 10 cm from the field edge, the model estimated the Monte Carlo H/D_{Rx} very well, with average percentage differences of −6.9 and 13.4% for the 160 and 140 MeV beams, respectively. This was the most important region because of the much higher H/D_{Rx} values compared to those beyond 10 cm. More specifically, between the two fields, the larger binned H/D_{Rx} values spanned from 0.13 to 1.28 mSv Gy^{-1} for 3 cm < r < 10 cm and were <0.13 mSv Gy^{-1} for $r \geq$ 10 cm. For 10 cm $\leq r \leq$ 20 cm, the model overestimated the Monte Carlo result by approximately a factor of 2. For r > 20 cm and to the bounds of the model training, where H/D_{Rx} was <0.03 mSv Gy^{-1}, the model overestimated the Monte Carlo result by roughly a factor of 2.5. For r > 49 cm, data were not shown because it was beyond the distance of the model training and the model systematically overestimated the Monte Carlo result. In that region, the internal neutron equivalent dose calculated previously by the Monte Carlo was negligible, at <0.001 mSv Gy^{-1}.

H_T/D_{Rx} values of the boy's fields were compared between the analytical model and Monte Carlo data (Figure 4). These data were summed with equal weighting between his fields of nominal energies of 140 and 160 MeV, both in the range of the lower energy component of the model. The model overestimated H_T/D_{Rx} of the Monte Carlo simulations for all organs and tissues. Thus, the model provided a conservative estimate of equivalent dose from

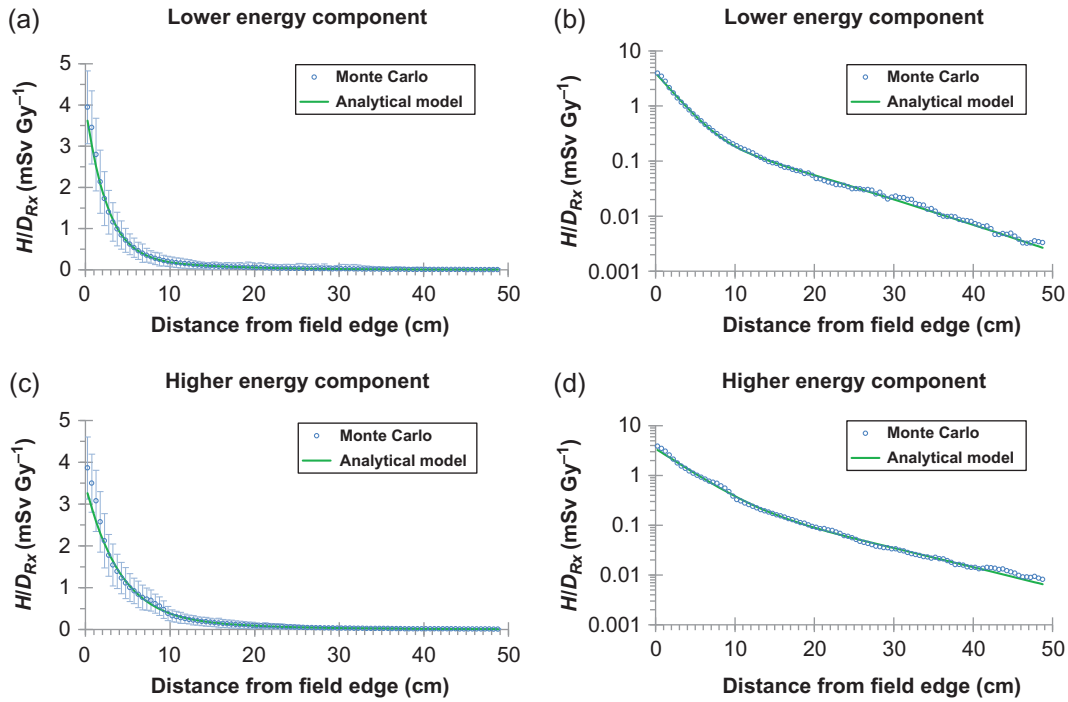

Figure 2. For the intracranial fields of the girl, H/D_{Rx} versus r for the analytical model (green line) and the training Monte Carlo data (blue circles). These plots are for internal neutrons only and were separated into the lower energy (**a** and **b**) and higher energy (**c** and **d**) components. The Monte Carlo data were from reference[11] and were averaged in 5-mm bins for viewing, with error bars representing one standard deviation of the mean in each bin.

Table 2. Fitted values of the parameters and their corresponding confidence intervals (reported at one standard deviation) for the lower and higher energy components of the analytical model. Also listed for each component are the *RMSD* values between the model and the Monte Carlo results for each component.

Lower energy component		Higher energy component	
Parameter	Value	Parameter	Value
α_{L1} (cm mSv Gy^{-1})	$1.080 \times 10^5 \pm 2.278 \times 10^5$	α_{H1} (cm mSv Gy^{-1})	$3.348 \times 10^5 \pm 8.164 \times 10^5$
μ_{L1} (cm)	-36.08 ± 9.946	μ_{H1} (cm)	-62.97 ± 18.86
σ_{L1} (cm)	9.553 ± 1.236	σ_{H1} (cm)	15.82 ± 2.330
α_{L2} (cm mSv Gy^{-1})	$3.739 \times 10^5 \pm 2.080 \times 10^6$	α_{H2} (cm mSv Gy^{-1})	$7.538 \times 10^5 \pm 8.640 \times 10^6$
μ_{L2} (cm)	-201.1 ± 109.3	μ_{H2} (cm)	-247.4 ± 262.0
σ_{L2} (cm)	47.24 ± 11.35	σ_{H2} (cm)	56.77 ± 26.39
RMSD (mSv Gy^{-1})	0.222	*RMSD* (mSv Gy^{-1})	0.225

secondary neutrons produced in the patient's body. The model results were within a factor of 2 of the Monte Carlo result for T having voxels with an average distance of <20 cm from the field edge. For organs farther from the field edge (i.e. lungs, stomach, liver, colon, bladder, and gonads), in which H_T/D_{Rx} values were <0.025 mSv Gy^{-1}, the model overestimated the internal neutron equivalent dose by a factor of 2–3, with the exception of the gonads for which the overestimation was <15%.

DISCUSSION

In this study, a computationally efficient and easy-to-implement analytical model was developed to estimate the equivalent dose from internal neutrons

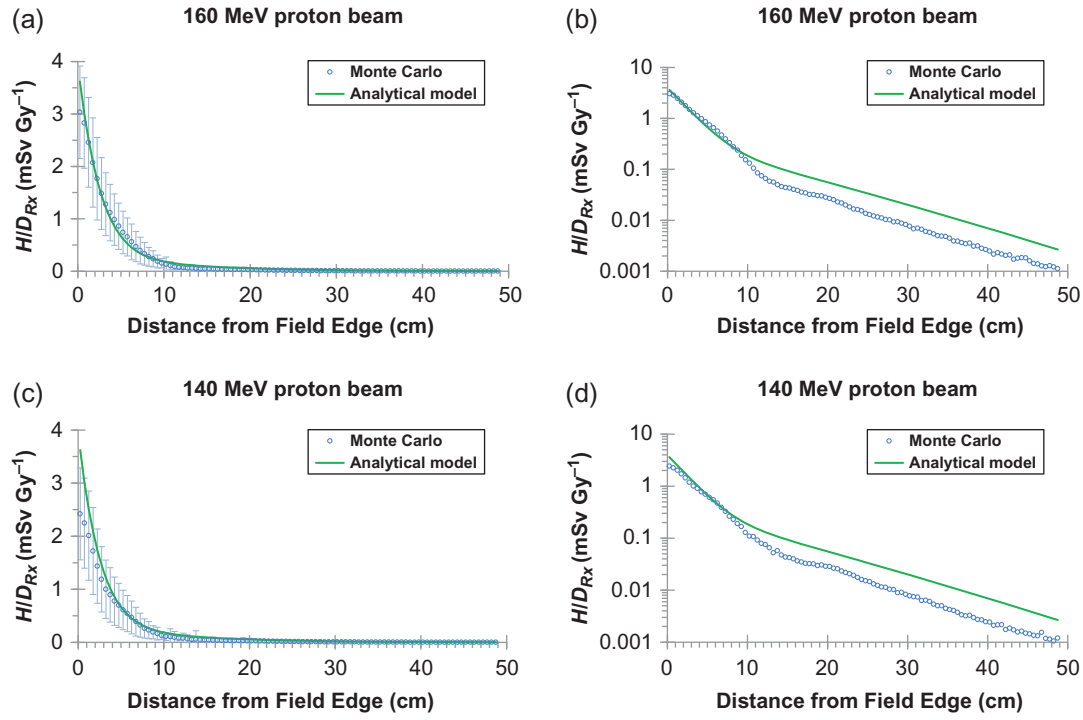

Figure 3. For intracranial fields of the boy, H/D_{Rx} versus r for the analytical model (green line) and the previously published Monte Carlo data (blue circles). These plots are for internal neutrons only and show the 160 MeV (**a** and **b**) 140 MeV (**c** and **d**) nominal energy beams, which are both in the condition of the model's lower energy component, i.e. $E \leq 160$ MeV. The Monte Carlo data were from reference[12] and were averaged in 5-mm bins for viewing, with error bars representing one standard deviation of the mean in each bin.

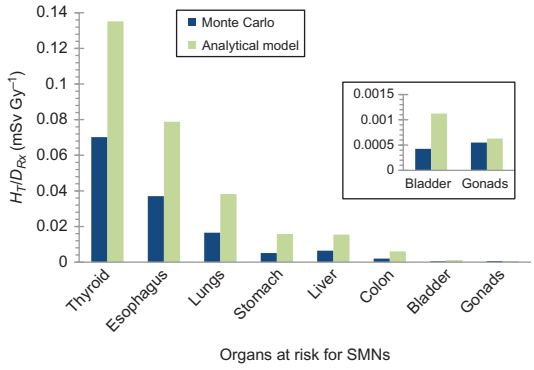

Figure 4. H_T/D_{Rx} determined by the analytical model (blue) and the Monte Carlo (light green) for the intracranial fields of a 10-year-old boy. The Monte Carlo data were from reference[12]. The inset zooms in on H_T/D_{Rx} of the bladder and gonads.

produced in proton therapy of pediatric intracranial tumors. The model was tested for the fields of a boy who received intracranial proton therapy and found to be most accurate from 3 cm to 10 cm from the field edge, adequate from 10 to 20 cm (within a factor of 2), and least accurate beyond 20 cm (systematic overestimation). However, the H/D_{Rx} values were very small (<0.03 mSv Gy^{-1}) in that region. Thus, this test showed that the model provided an adequate but conservative estimation of internal neutron equivalent dose throughout the boy's body.

H/D_{Rx} was found to be small beyond 10 cm. Specifically, the modeled lower energy and higher energy components of H/D_{Rx} at 10 cm were 0.19 and 0.38 mSv Gy^{-1}, respectively. These values correspond to 9.3 and 18.7 mSv for a 54 Gy-RBE proton treatment. Equivalent doses <50 mSv are below the quantity for which the carcinogenic dose–response relationship has known statistical significance[27]. Thus, for general purposes in pediatric intracranial proton therapy, the recommended application of this H/D_{Rx} model in pediatric intracranial proton therapy may be for r between 3 and 49 cm. For estimating the risk of SMNs in pediatric intracranial proton therapy, however, it is reasonable to consider the equivalent dose from internal neutrons beyond 10 cm from the field edge to be insignificant.

As a figure of merit, H_T/D_{Rx} values were compared in organs and tissues at risk for SMNs estimated by the analytical model versus those calculated in previously published Monte Carlo simulations. H_T/D_{Rx} calculated by the model and the Monte Carlo simulations differed by less than a factor of 2 for organs and tissues close in close proximity to the fields. A factor of 2 uncertainty would be unacceptable for therapeutic doses. However, for out-of-field neutron doses, for which other large uncertainties exist—e.g. radiation weighting factor and RBE[28–31], dose and dose rate effectiveness factor[32], and measurement uncertainties in validating the Monte Carlo[33–36]—a factor of 2 uncertainty is acceptable[7]. On this basis, the application of this analytical model to evaluate out-of-field dose from internal neutrons may be considered a sizable step forward from the current clinical practice of disregarding these doses. For organs far from the field edge, e.g. the stomach and colon, inaccuracy of the model increased by more than a factor of 2. However, in these far out-of-field organs the absolute equivalent doses from internal neutrons were small. The modeled H_T/D_{Rx} values of the analytical model were greater than those of the Monte Carlo in all organs and tissues. It was notable that one of the boy's beams was of lower nominal energy than the girl's beams that were used to train the model and internal neutron equivalent dose increased with proton beam energy. Data were lacking in the literature for additional comparison for the higher energy component of the model. To address this, the H_T/D_{Rx} in the thyroid calculated by the analytical model was compared to that of a roughly similar $E = 168.2$ MeV field of an 8-year-old girl in a study by Zacharatou Jarlskog *et al.*[15]. The result of the analytical model, at 0.70 mSv Gy^{-1}, was higher than their result, at 0.31 mSv Gy^{-1}. This difference may have been attributable to a discrepancy in the distance of the thyroid from the field edge or their differing definition of radiation weighting factor compared to that of the previous Monte Carlo study on which this analytical model was trained.

For higher energy fields, the model can also be compared to pencil-beam scanning measurements. Specifically, Stolarczyk *et al.*[33] very recently measured the neutron dose equivalent in a water phantom for a proton field of 10 cm × 10 cm with a nominal range of 20 cm and modulation of 10 cm (i.e. 16 layers of energies between 116 and 171 MeV). Their neutron dose equivalent values at 3.6, 8.6 and 23.6 cm from the field edge (given a field width of 113.7 mm at isocenter) were ~1.73, 0.77 and 0.07 mSv Gy^{-1}, respectively. They approximated the uncertainty at 30% for their polyallyldiglycol carbonate-based ($C_{12}H_{18}O_7$) track-etched dosimeters. The corresponding neutron equivalent dose values estimated by the analytical model developed in this study at these r were 1.50, 0.51 and 0.06 mSv Gy^{-1}, respectively. Thus, for their most similar field, the analytical model results were in very good agreement with their measured data.

The strength of the analytical model is its fast application to account for stray neutron radiation in proton therapy, in which internal neutrons contribute to the potential risk of late effects, for example, radiation-induced necrosis and cancer. The newest proton therapy facilities have adopted pencil-beam scanning and some older facilities are being retrofitted for this delivery technique. As pencil-beam scanning largely mitigates external neutron production, internal neutron doses will emerge as the stray radiation of primary concern for patients receiving proton therapy. For example, in the absence of external neutrons, the internal neutrons generated from the 160 MeV proton field accounted for ~25 and 50% of the equivalent dose at 3 and 15 cm from the field edge, respectively. Thus, quantifying the internal neutron dose has become all the more important.

The model did not account for external neutrons, which vary greatly by beam characteristics, facility design and treatment delivery apparatus. To account for neutrons produced outside the patient, for example, in treatment units for which the fields are partially or fully shaped by scattering or modulating components during delivery, a separate model should be applied. One model that had been developed extensively to estimate patients' external neutron exposures was that of Schneider *et al.*[18]. These analytical models, combined with the proton dose calculated by the clinical TPS and extended anatomical imaging and organ delineation[25], have the potential for fast generation of a whole-body dosimetric map with limited computational overhead. Fast full body dosimetry may enable the estimation of long-term side effects for clinical decisions or the relating of dose and effects for epidemiological studies, most importantly for pediatric patients[37–39].

The chief limitation of this study was that the model is only applicable for similar pediatric intracranial tumors. For different treatment sites, the double-Gaussian model may be valid but would require re-fitting of its parameters. Future studies should expand the model to become more broadly encompassing to include other treatment sites and various energies of beams and sizes of irradiated volumes. The latter would account for spread out Bragg peaks and aperture sizes. Alternatively, a mechanistic model that accounts for energy and irradiated volume size would be more robust and should be explored. A second important limitation of the study was that only one patient's Monte Carlo simulations were available for testing of the model. Another limitation was that the validation fields were in the range of the lower energy component only and not the higher energy component. For these

reasons, although the results of the analytical model were compared to others' Monte Carlo and measured data, the testing of the model may be considered preliminary.

In conclusion, an analytical model was trained for a child receiving intracranial proton therapy and tested to adequately, and somewhat conservatively, estimate out-of-field internal neutron dose for similar fields in a second child. The model was most accurate within 10 cm of the treatment fields, where the internal neutron dose contributes the most to overall exposures. For most modern proton therapy machines capable of spot scanning, internal neutrons are responsible for the bulk of stray radiation exposures to patients. Because these secondary neutrons are generated in patients' bodies, this model may be applied for similar proton therapy fields to estimate internal neutron equivalent dose, regardless of treatment unit design or clinical environment. This study also demonstrated the feasibility of using analytical models rather than complicated and computationally expensive Monte Carlo simulations to generate estimates of neutron doses in patients receiving proton therapy.

ACKNOWLEDGEMENTS

The scientific counsel of John Eley, Jatinder Saini, Robert Stewart and Wayne Newhauser was gratefully received.

FUNDING

This work was supported by the Fogarty International Center [award K01TW008409]; the Naef K. Basile Cancer Institute; and the Portland Chapter of the Achievement Rewards for College Scientists. The content is solely the responsibility of the authors and does not necessarily represent the official views of the sponsors.

REFERENCES

1. Jermann, M. *Patient statistics per end of 2016*. Particle Therapy Co-Operative Group (2017). Available on https://www.ptcog.ch/index.php/patient-statistics.
2. Ladra, M. M., MacDonald, S. M. and Terezakis, S. A. *Proton therapy for central nervous system tumors in children*. Pediatr. Blood Cancer **65**, e27046 (2018).
3. Armstrong, G. T., Stovall, M. and Robison, L. L. *Long-term effects of radiation exposure among adult survivors of childhood cancer: results from the Childhood Cancer Survivor Study*. Radiat. Res. **174**, 840–850 (2010).
4. Armstrong, G. T., Liu, Q., Yasui, Y., Neglia, J. P., Leisenring, W., Robison, L. L. and Mertens, A. C. *Late mortality among 5-year survivors of childhood cancer: a summary from the Childhood Cancer Survivor Study*. J. Clin. Oncol. **27**, 2328–2338 (2009).
5. Diallo, I. *et al. Frequency distribution of second solid cancer locations in relation to the irradiated volume among 115 patients treated for childhood cancer*. Int. J. Radiat. Oncol. **74**, 876–883 (2009).
6. Brenner, D. J., Curtis, R. E., Hall, E. J. and Ron, E. *Second malignancies in prostate carcinoma patients after radiotherapy compared with surgery*. Cancer **88**, 398–406 (2000).
7. Newhauser, W. D. and Durante, M. *Assessing the risk of second malignancies after modern radiotherapy*. Nat. Rev. Cancer **11**, 438–448 (2011).
8. Taddei, P. J. *et al. Low- and middle-income countries can reduce risks of subsequent neoplasms by referring pediatric craniospinal cases to centralized proton treatment centers*. Biomed. Phys. Eng. Express **4**, 025029 (2018).
9. Matsumoto, S., Koba, Y., Kohno, R., Lee, C., Bolch, W. E. and Kai, M. *Secondary neutron doses to pediatric patients during intracranial proton therapy: Monte Carlo simulation of the neutron energy spectrum and its organ doses*. Health Phys. **110**, 380–386 (2016).
10. Geng, C., Moteabbed, M., Xie, Y., Schuemann, J., Yock, T. and Paganetti, H. *Assessing the radiation-induced second cancer risk in proton therapy for pediatric brain tumors: the impact of employing a patient-specific aperture in pencil beam scanning*. Phys. Med. Biol. **61**, 12–22 (2016).
11. Taddei, P. J., Mahajan, A., Mirkovic, D., Zhang, R., Giebeler, A., Kornguth, D., Harvey, M., Woo, S. and Newhauser, W. D. *Predicted risks of second malignant neoplasm incidence and mortality due to secondary neutrons in a girl and boy receiving proton craniospinal irradiation*. Phys. Med. Biol. **55**, 7067–7080 (2010).
12. Taddei, P. J., Mirkovic, D., Fontenot, J. D., Giebeler, A., Zheng, Y., Kornguth, D., Mohan, R. and Newhauser, W. D. *Stray radiation dose and second cancer risk for a pediatric patient receiving craniospinal irradiation with proton beams*. Phys. Med. Biol. **54**, 2259–2275 (2009).
13. Newhauser, W. D. *et al. The risk of developing a second cancer after receiving craniospinal proton irradiation*. Phys. Med. Biol. **54**, 2277–2291 (2009).
14. Fontenot, J., Taddei, P. J., Zheng, Y., Mirkovic, D., Jordan, T. and Newhauser, W. D. *Equivalent dose and effective dose from stray radiation during passively scattered proton radiotherapy for prostate cancer*. Phys. Med. Biol. **53**, 1677–1688 (2008).
15. Zacharatou Jarlskog, C., Lee, C., Bolch, W. E., Xu, X. G. and Paganetti, H. *Assessment of organ specific neutron equivalent doses in proton therapy using computational whole-body age-dependent voxel phantoms*. Phys. Med. Biol. **53**, 693–717 (2008).
16. Gallagher, K. J. and Taddei, P. J. *Independent application of an analytical model for secondary neutron equivalent dose produced in a passive-scattering proton therapy treatment unit*. Phys. Med. Biol. **63**, 15NT04 (2018).
17. Eley, J., Newhauser, W. D., Homann, K., Howell, R., Schneider, C., Durante, M. and Bert, C. *Implementation of an analytical model for leakage neutron equivalent dose in a proton radiotherapy planning system*. Cancers **7**, 427–438 (2015).
18. Schneider, C., Newhauser, W. D. and Farah, J. *An analytical model of leakage neutron equivalent dose for*

passively-scattered proton radiotherapy and validation with measurements. Cancers **7**, 795–810 (2015).
19. Pérez-Andújar, A., Zhang, R. and Newhauser, W. *Monte Carlo and analytical model predictions of leakage neutron exposures from passively scattered proton therapy*. Med. Phys. **40**, 121714 (2013).
20. Zhang, R., Pérez-Andújar, A., Fontenot, J. D., Taddei, P. J. and Newhauser, W. D. *An analytic model of neutron ambient dose equivalent and equivalent dose for proton radiotherapy*. Phys. Med. Biol. **55**, 6975–6985 (2010).
21. Chang, A. L., Yock, T. I., Mahajan, A., Hill-Kaiser, C., Keole, S., Loredo, L., Cahlon, O., McMullen, K. P., Hartsell, W. and Indelicato, D. J. *Pediatric proton therapy: patterns of care across the United States*. Int. J. Part. Ther. **1**, 357–367 (2014).
22. International Commission on Radiation Units and Measurements. *Prescribing, recording, and reporting proton-beam therapy*. ICRU Report 78. J. ICRU (2007).
23. Hirayama, S. *et al. Evaluation of the influence of double and triple Gaussian proton kernel models on accuracy of dose calculations for spot scanning technique*. Med. Phys. **43**, 1437–1450 (2016).
24. Taddei, P. J., Jalbout, W., Howell, R. M., Khater, N., Geara, F., Homann, K. and Newhauser, W. D. *Analytical model for out-of-field dose in photon craniospinal irradiation*. Phys. Med. Biol. **58**, 7463–7479 (2013).
25. Gallagher, K. J., Tannous, J., Nabha, R., Feghali, J. A., Ayoub, Z., Jalbout, W., Youssef, B. and Taddei, P. J. *Supplemental computational phantoms to estimate out-of-field absorbed dose in photon radiotherapy*. Phys. Med. Biol. **63**, 025021 (2018).
26. International Commission on Radiological Protection. 1990 Recommendations of the International Commission on Radiological Protection. ICRP Publication 60. *Ann. ICRP* 21 (1991).
27. Brenner, D. J. *et al. Cancer risks attributable to low doses of ionizing radiation: assessing what we really know*. Proc. Natl. Acad. Sci. USA **100**, 13761–13766 (2003).
28. Kuhne, W. W., Gersey, B. B., Wilkins, R., Wu, H., Wender, S. A., George, V. and Dynan, W. S. *Biological effects of high-energy neutrons measured in vivo using a vertebrate model*. Radiat. Res. **172**, 473–480 (2009).
29. Hollander, C. F., Zurcher, C. and Broerse, J. J. *Tumorigenesis in high-dose total body irradiated rhesus monkeys—a life span study*. Toxicol. Pathol. **31**, 209–213 (2003).
30. Wolf, C., Lafuma, J., Masse, R., Morin, M. and Kellerer, A. M. *Neutron RBE for induction of tumors with high lethality in Sprague-Dawley rats*. Radiat. Res. **154**, 412–420 (2000).
31. Grahn, D., Lombard, L. S. and Carnes, B. A. *The comparative tumorigenic effects of fission neutrons and cobalt-60 gamma rays in the B6CF1 mouse*. Radiat. Res. **129**, 19–36 (1992).
32. National Research Council of the National Academies. *Health Risks from Exposure to Low Levels of Ionizing Radiation: BEIR VII—Phase 2*. The National Academies Press (2006) ISBN 0 309 530407.
33. Stolarczyk, L. *et al. Dose distribution of secondary radiation in a water phantom for a proton pencil beam—EURADOS WG9 intercomparison exercise*. Phys. Med. Biol. **63**, 085017 (2018).
34. Howell, R. M. and Burgett, E. A. *Secondary neutron spectrum from 250-MeV passively scattered proton therapy: measurement with an extended-range Bonner sphere system*. Med. Phys. **41**, 092104 (2014).
35. Wroe, A., Rosenfeld, A. and Schulte, R. *Out-of-field dose equivalents delivered by proton therapy of prostate cancer*. Med. Phys. **34**, 3449–3456 (2007).
36. Fontenot, J. D., Newhauser, W. D. and Titt, U. *Design tools for proton therapy nozzles based on the double-scattering foil technique*. Radiat. Prot. Dosimetry **116**, 211–215 (2005).
37. Berrington de Gonzalez, A. *et al. A clarion call for large-scale collaborative studies of pediatric proton therapy*. Int. J. Radiat. Oncol. Biol. Phys. **98**, 980–981 (2017).
38. Stokkevåg, C. H., Schneider, U., Muren, L. P. and Newhauser, W. D. *Radiation-induced cancer risk predictions in proton and heavy ion radiotherapy*. Phys. Medica **42**, 259–262 (2017).
39. Newhauser, W. D., Berrington de Gonzalez, A., Schulte, R. and Lee, C. *A review of radiotherapy-induced late effects research after advanced technology treatments*. Front. Oncol. **6**, 13 (2016).